J Mater Sci: Mater Electron (2022) 33:23404–23417

# Thin films of graphene decorated with $NiS_2$ hybrid sensor for detection of $NO_2$ gas

R. Sakthivel[1], A. Geetha[2], B. A. Anandh[1], S. Mohankumar[1], and J. Dineshkumar[3,*]

[1] Department of Electronics, PSG College of Arts & Science, Civil Aerodrome Post, Coimbatore 641 014, Tamilnadu, India
[2] Department of Chemistry, Hindusthan College of Arts and Science, Hindusthan Gardens (Behind Nava India), Avinashi Road, Coimbatore 641 028, Tamilnadu, India
[3] Department of Electronics and Communication Systems, VLB Janakiammal College of Arts and Science, Kovaipudur, Coimbatore 641 042, Tamilnadu, India

**Received:** 25 March 2022
**Accepted:** 7 September 2022

## ABSTRACT

Here, we demonstrate the improved $NO_2$ gas-sensing properties based on graphene-decorated $NiS_2$ thin film. The grown $NiS_2$ thin film, graphene was spread over $NiS_2$ thin film by chemical vapour deposition (CVD) method. The formation of several p–n heterojunctions is greatly affected by the current–voltage relation of graphene-decorated $NiS_2$ thin film due to p-type and n-type nature of graphene and $NiS_2$, respectively. Initially with graphene decoration on $NiS_2$ thin film, current decreases in comparison to $NiS_2$ thin film, whereas depositing graphene film on glass substrate, current increases drastically. The $NO_2$ gas sensor device is fabricated and its basic characteristics are systematically investigated. The incorporated graphene improves the $NO_2$ sensing response of 97% with compared to bare $NiS_2$ sensor (29%) at 100 ppm $NO_2$ concentration with a practical detection limit below 0.2 ppm. In addition, the recovery time was shortened to a few seconds and the excellent repeatability. This work may provide a promising and practical method to mass produce room-temperature $NO_2$ gas sensors for real-time environment monitoring due to its simple fabrication process, low cost, and practicality. The high-sensing response of $NiS_2$/graphene is attributed to the formation and modulation of p–n heterojunction at the interface of graphene and $NiS_2$. In addition, the presence of active sites graphene surface also enhances the sensing response.

---

Address correspondence to E-mail: dineshpsgcas2@gmail.com

https://doi.org/10.1007/s10854-022-09101-z

## 1 Introduction

Gas sensors are generally understood as providing a measurement of the concentration of some analyte of interest, such as CO, $CO_2$, NO*x*, $SO_2$, without at this point dwelling on the plethora of underlying approaches such as optical absorption, electrical conductivity, electrochemical (EC), and catalytic bead. Gas sensors are devices that help us understand the amount of gas in the environment and the natural state of its movement. Gas sensors reveal the amount of gas in the environment and the nature of the gas composition with electrical signals and can provide its change [1–4]. Currently, environmental pollution has created huge trouble due to its harmful effects on all living organisms. Nitrogen dioxide ($NO_2$) is one of the most known air pollutant in the environment whose major emission is from industrial waste, automobile by-products, and power plants [1–3]. Further, the formation of acid rain takes place when $NO_2$ interacts with water molecules in the atmosphere, resulting in serious harm to the ecosystem [5]. In addition, the continued inhalation of $NO_2$ to gives rise to throat irritation, lung infections and reduces the capability of the respiratory system [6–8]. Therefore, the enlargement of highly sensitive and selective $NO_2$ gas sensors has become an utmost necessity for timely detection of the harmful gas even at extremely low concentration around 1 ppm. To suffice the demand of efficient gas sensors, the need of metal oxide semiconductor based gas sensors for precise detection of $NO_2$ gas emerges [9, 10]. The demand for highly sensitive and reliable chemiresistive-based $NO_2$ sensor has been increasing over the last few years. In response to this demand, huge effort has been made to develop and design high surface area electrodes with good physico-chemical properties [11]. Numerous materials belonging to transition metal oxides/sulfides, doped metal oxides, metal hydrides, and polymeric materials have been used for fabricating sensing materials [12–16]. Among these materials, nickel sulphides are considered to be productive semiconducting materials for sensor applications not only because of their chemical sensitivity to liquid as well as major gases, its low-cost, nontoxic nature, high chemical stability and greater natural abundance. Sulfides of various transition metals show interesting electrical and optical properties such as semiconductivity, luminescence, gas sensors and photoconductivity. $NiS_2$ demonstrates excellent potential for $NO_2$ identification at room temperature [17]. $NiS_2$ has also been emerging as a promising material, which also shows great potential because of their high conductivity [18]. However, improving the sensing performances of nickel sulfides is still a challenge. Therefore, the present approach for nickel sulfides is to increase the electronic conductivity. On the other hand, carbon nanotubes and graphene have been extensively studied because of their exceptional physical characteristics, such as their large surface areas, exceptional chemical stabilities, outstanding electronic properties and potential applications in sensors. The introduction of graphene and other carbon support materials during the preparation of nickel sulfides has proven to be an effective strategy to prevent the aggregation of nickel sulfide particles and provide more effective interconnected networks for electron transport [19]. As widely reported in the literature, graphene prepared from multiple approaches that include mechanical exfoliation, chemical vapor deposition, and epitaxial growth has shown a low limit of detection, small noise, and good reversibility [20, 21]. Recently, $NiS_2$ has been reported as a good material for gas sensing [22], since its hybridization with graphene to form composite/hybrid materials results in high sensitivity due to synergistic effects and solves the problem of slow graphene-only sensor recovery [23–27]. In addition, direct deposition of $NiS_2$ on graphene using high-temperature chemical vapor deposition (CVD) affords sensors with increased thermal stability. Moreover, $NiS_2$ with preferentially exposed active edge sites has been reported to be more active than that with exposed basal planes. Hence, we herein use thermal CVD to deposit $NiS_2$ on graphene, utilizing the fabricated hybrid materials to detect $NO_2$ gas at very low concentration and determining the properties of the prepared sensor. Furthermore, the structure, morphology and sensing characteristics of the hybrid composites were investigated in detail. The $NiS_2$ gas sensor responded with a 28% change upon being exposed to 100 ppm of $NO_2$, while the response of the $NiS_2$/graphene device reached 97% when exposed to the same $NO_2$ concentration. Moreover, the fabricated sensor showed long term stability and high selective response towards $NO_2$ gas than compared with other gaseous species. The improved sensing mechanism of the proposed sensor was also discussed in detail. The synthetic strategy reported here may provide new opportunities to improve the sensing properties of $NiS_2$/graphene composites.

## 2 Experimental details

### 2.1 Materials

Nickel sulphide thin films were prepared from aqueous solution of nickel chloride ($NiCl_2$) and sodium thisulphate ($Na_2S_2O_3.5H_2O$) as sources of $Ni^{2+}$ and $S_2^-$ ions respectively. All the chemicals used were of analytical grade and all the solutions were prepared in de-ionized water. Ammonia ($NH_3$) solution was used as a complexing agent during the deposition.

### 2.2 Fabrication of pristine $NiS_2$ and $NiS_2$/graphene thin films

Based on the previous literature work, the bare graphene was synthesized from graphite powder using a hydrothermal method [28]. In a typical synthesis of $NiS_2$, the original molar ratio between $NiCl_2$ $2H_2O$ and $Na_2S_2O_3{\cdot}5H_2O$ was selected to be 1:3. $NiCl_2.2H_2O$ (0.28 g, 0.001 M) was dissolved in deionized water (30 mL). The chelating agent, triethanolamine (12 mL ≈ 0.003 M), was added to the solution. NaOH (1.0 g, 0.025 M) was added to keep the pH value at about 10. After mixing for 5 min under stirring, $Na_2S_2O_3{\cdot}5H_2O$ (0.78 g, 0.003 M) was added to the mixture, and the system finally formed a blue, transparent solution. In a typical synthesis of $NiS_2$, the original molar ratio between $NiCl_2$ and $Na_2S_2O_3.5H_2O$ was selected to be 1:3. $NiCl_2$ (0.30 g, 0.001 M) was dissolved in deionized water (30 mL). The chelating agent, triethanolamine (12 mL ≈ 0.003 M), was added to the solution. $NH_3$ (0.05 M) was added to keep the pH value at about 9. In the standard horizontal configuration, a quartz tube about 1 m long with a diameter of 2–5 cm is used. The heating resistance is placed around the quartz tube. The solution was ionized by an ultrasonic generator of 1.7 MHz frequency, produced aerosol was carried directly to the heated substrates using compressed air as carrier gas in a flow rate of 5 L/min. The number of spray cycles was optimized to six. After that the deposited FTO substrate was taken out and dried in a dessicator under low vacuum (approx. $10^{-2}$ mbar) for 24 h. The as-synthesized films were named as pure $NiS_2$. In $NiS_2$/graphene film, 0.5 g of graphite powder was mixed with $NiS_2$ precursor solution and same experiment was carried out. Finally, the dried FTO film was named as $NiS_2$/graphene film. Figures S1 and S2 show the schematic representation for the synthesis process of graphene and $NiS_2$/graphene hybrid thin film. Figure S3 shows the photograph image of fabricated thin films.

### 2.3 Fabrication of gas sensor set up

Figure 1 shows the fabrication process of a gas sensor device. Alumina plates with silver interdigitated electrodes were used as substrates. The width and interspacing of the electrodes were 0.3 mm and 0.15 mm, respectively. The electrical response of the sensors towards change in LPG gas was recorded using an in-house built controlled environmental chamber. The gas-sensing measurements were performed in a mass flow controlled vacuum chamber which periodically allowed and stopped the flow of gas. Two sides of the electrode were connected to a computer controlled source-meter (Keithley-237), for measurement of the gas sensing curves at room temperature. The sensor response is calculated using $S\ (\%) = \Delta R/R \times 100$, where $\Delta R$ is a difference between the gas and air resistance; $R$ is the gas resistance. The response time was defined as the moment when the resistance of the sensor reached 90% of its final value in the presence of the target gas, and the recovery time was defined as the time needed for the resistance to reach 90% of its initial value after

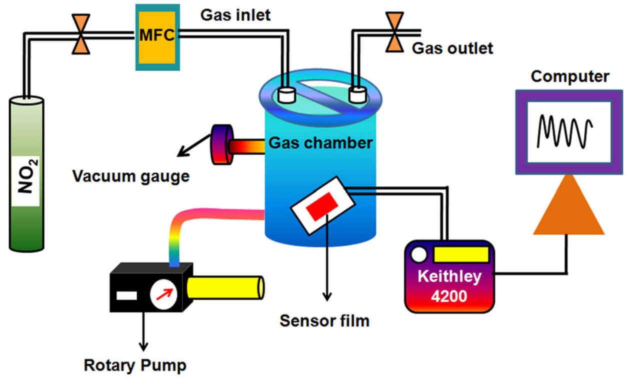

**Fig. 1** Schematic representation of the resistive type gas sensor setup

gas stoppage. Figure S4a Photograph of gas sensor set up and b $NiS_2$ sensor film (Final device), respectively.

## 3 Results and discussion

### 3.1 XRD analysis

The phase and crystalline structure of the sensor samples were analyzed by XRD method. Figure 2 shows the XRD pattern of graphene, $NiS_2$, and $NiS_2$/graphene films, respectively. The strong diffraction peak at 26.97° is attributed to the (002) planes of graphene [29]. As shown in Fig. 2, the peaks appeared at $2\theta = 26.8°$, 31.3°, 36.5°, 38.1°, 45.3°, 49.1°, 52.3°, 53.4°, 58.5°, 61.2°, and 67.0° corresponding to the (111), (200), (211), (220), (221), (311), (023), (321), and (400) planes, respectively, which can be clearly indexed to cubic pyrite $NiS_2$ with lattice parameters of $a = 5.67$ Å, which is consistent with the reported data for $NiS_2$ (JCPDS # 11-99).

The intensity of (200) diffraction peaks is relatively higher than the conventional value, indicating that the (200) plane of $NiS_2$ tends to be preferentially oriented in the experimental system. The presence of (002) plane along with $NiS_2$ diffraction in the composite samples demonstrate that nanocomposites of $NiS_2$ and graphene was formed. Raman spectra were further carried out to identify the functional groups and graphene hybridization with $NiS_2$ crystal matrix.

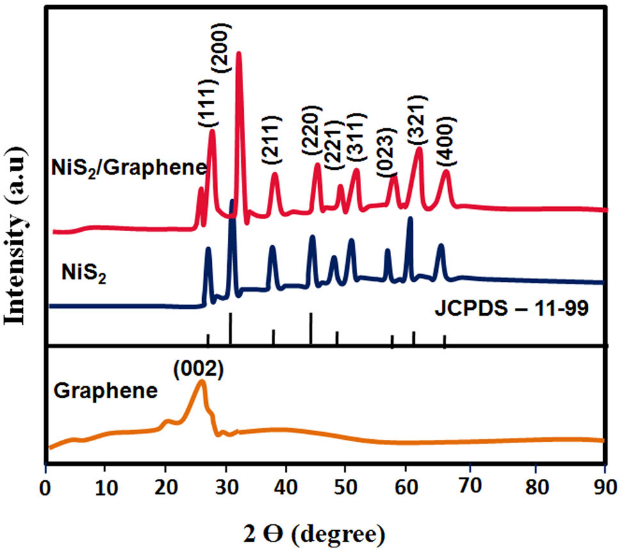

**Fig. 2** X-ray diffraction pattern of the sensor samples

### 3.2 FTIR and Raman analysis

Fourier transform infrared spectroscopy (FTIR) is employed to clarify the functional groups of graphene, $NiS_2$ and the $NiS_2$/graphene composite. As shown in Fig. 3a, the peak at 625 $cm^{-1}$ can be attributed to the Ni–S stretching vibration. The multiple peaks at 700–1150 $cm^{-1}$ can be assigned to the sulfate groups, while the sharp peaks at 3445 and 1614 $cm^{-1}$ can be ascribed to the O–H stretching and water bending, respectively. For the graphene spectrum, the intense peak located at 1614 $cm^{-1}$ can be attributed to the aromatic C=C (stretching), and the very weak peak located at 1125 $cm^{-1}$ corresponds to the C–O stretching. In contrast, the absence of a C=O peak around 1715 $cm^{-1}$ indicates the insignificant amount of oxidation of graphene. Raman Spectroscopy is a very powerful tool for analyzing the properties of carbon and other two-dimensional materials. It also used to confirm the successful hybridization of carbon with TMDs. The Raman spectra of pure graphene, $NiS_2$, and $NiS_2$/graphene composite samples are shown in Fig. 3b. Typically, the $NiS_2$ film exhibits two Raman characteristic peaks at about 280.6 $cm^{-1}$ and 490.9 $cm^{-1}$, corresponding to the $A_{1g}$ and $E_{2g}$ modes, respectively [30, 31]. The ratio of the D to G band in the composites is larger than that of graphene due to increased lattice disorder and compared to pure graphene, the D and G bands red-shift because of electron transfer at the interface. The combination Raman modes of $NiS_2$ and graphene in the composite films further confirms that successful formation heterostructure composite between $NiS_2$ and graphene.

### 3.3 Morphological studies

The morphology and structure of the $NiS_2$/graphene were investigated by SEM and TEM. Typical morphological information of the as grown films is shown in Fig. 4. A sheet-like shape with an average diameter of roughly 2–3 µm can be seen in a SEM image of pure graphene (Fig. 4a). The pure $NiS_2$ sample has irregularly shaped nanograins that are consistently adorned on the surface of the graphene nanosheet in the $NiS_2$/graphene film, whereas the $NiS_2$/graphene film has uniformly decorated graphene nanosheets (Fig. 4c). In the TEM image, the crumble type sheet like form of graphene was also discovered (Fig. 4d). The surface of graphene

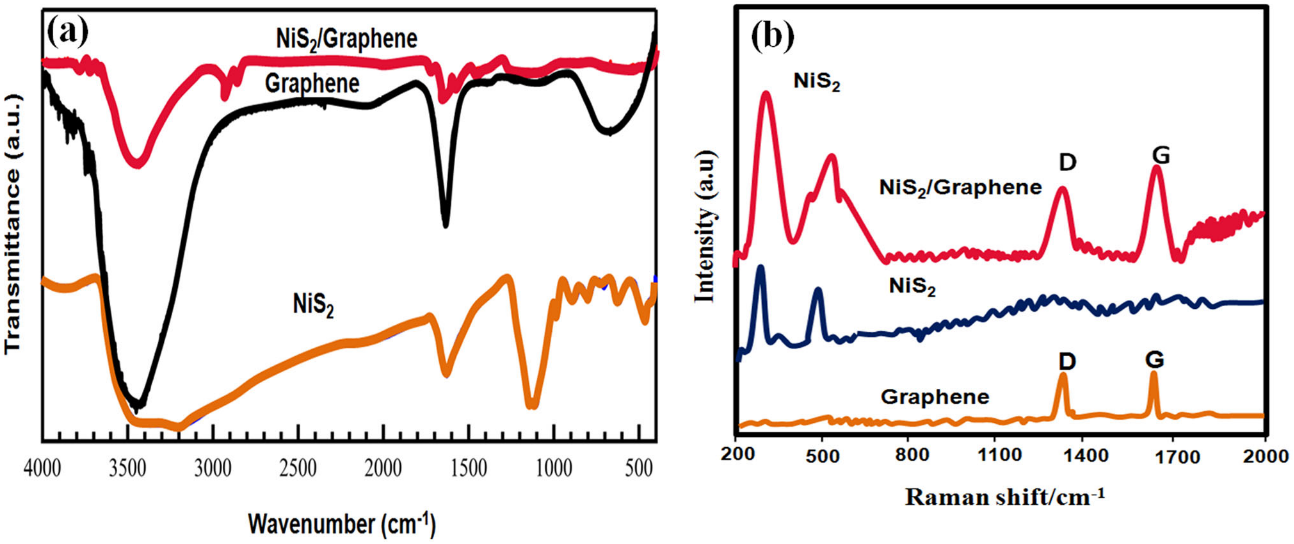

**Fig. 3** **a** FTIR and **b** Raman spectra of the sensor samples

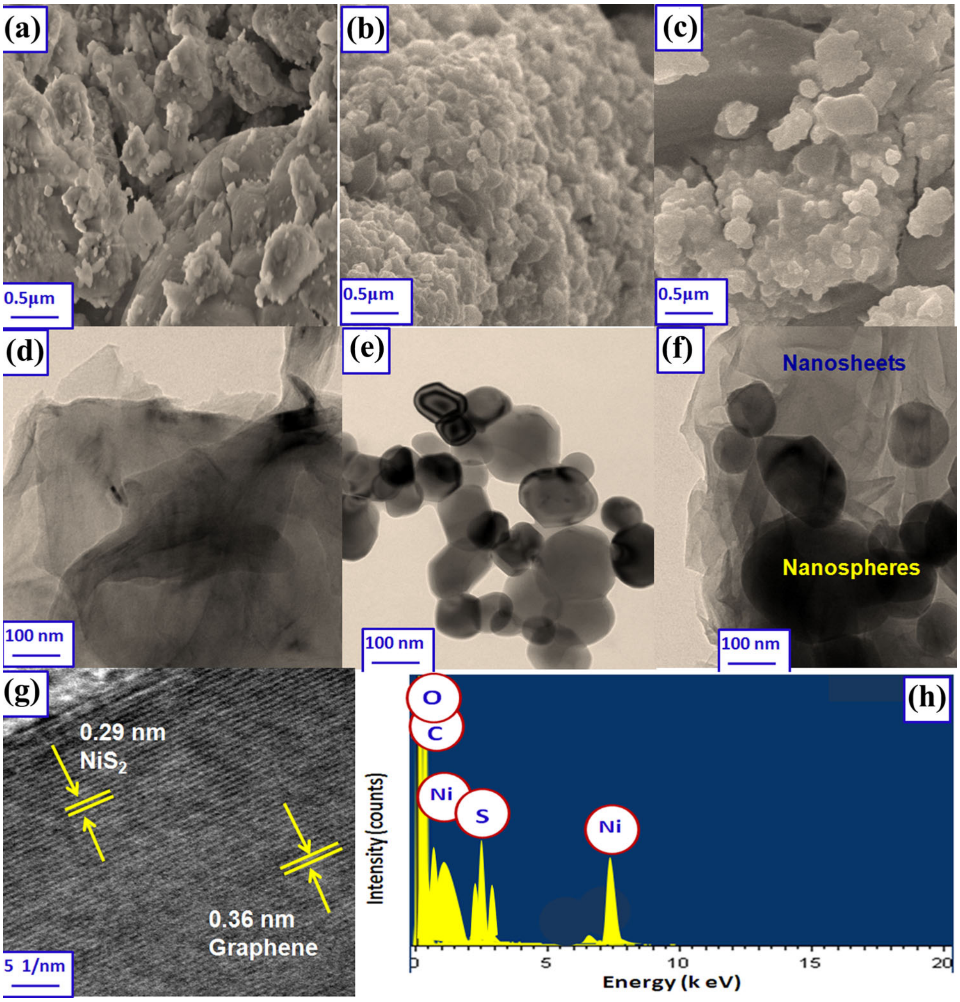

**Fig. 4** SEM images of **a** graphene, **b** NiS$_2$, **c** NiS$_2$/G, TEM images of **d** graphene, **e** NiS$_2$, **f** NiS$_2$/G, **g** HRTEM of NiS$_2$/G and **h** EDS of NiS$_2$/G

nanosheets was uniformly adorned with spherical shaped NiS$_2$ nanoparticles with diameters in the range of 30–35 nm (Fig. 4e, f). We used high-resolution transmission electron microscopy (HR-TEM) to examine the microstructure of the NiS$_2$/graphene composite thin film to determine its definite lattice structure (Fig. 4g). As demonstrated in Figure, NiS$_2$ and graphene are clearly differentiated from one another, with lattice spacing distances of 0.29 nm and 0.36 nm, respectively, corresponding with NiS$_2$ and graphene lattice spacing. The chemical compositions of the as developed NiS$_2$/graphene nanocomposites were also evaluated by EDS analysis (Fig. 4h), which confirmed the existence of C, S, and Ni. Carbon, sulphur, and nickel content (wt%) in NiS$_2$/graphene are 54.12%, 18.16%, and 27.72%, respectively.

## 3.4 Surface area analysis

The gas-sensing characteristics of nanostructured materials are inherently connected with the available surface area and porosity. The specific surface area and porosity of NiS$_2$ and NiS$_2$/graphene samples were investigated by N$_2$ adsorption–desorption isotherms. The isotherms of these two samples are shown in Fig. 5a. Both samples display type IV isotherms with small hysteresis loop [32–35]. These results indicate that the pore volumes are supplied by mesopores in these samples, thus, providing efficient channels for mass transport. The presence of mesoporous—structure was apparent and confirmed by Brunauer–Emmett–Teller (BET) data, which showed specific surface areas of 49.7 and 102.8 m$^2$/g for NiS$_2$ and NiS$_2$/graphene, respectively. Figure 5b depicts the Barrett–Joyner–Halenda (BJH) results. The NiS$_2$ and NiS$_2$/graphene pore pore diameters are 12.89 and 19.12 nm, respectively, confirming the presence of a mesoporous—structure. However, the NiS$_2$/graphene film exhibiting a high surface area (102.8 m$^2$/g) with porous structure has a large amount of surface active sites for the oxygen adsorption and reaction with detected NO$_2$ gas molecules. This may enhance the free electron exchange between the surface adsorbed species of the surface and the bulk of the NiS$_2$ film. Therefore, the sensor having a larger effective surface area can supply a larger amount of surface adsorbed species (O$_2^-$, O$^-$ and O$_2^-$, etc.), resulting in larger changes in the electrical conductivity of the sensor and eventually in obtaining a higher sensitivity.

## 3.5 XPS analysis

The elemental composition and oxidation states of the NiS$_2$/graphene hybrid composite were further analyzed by XPS. As shown in Fig. 6a, the full survey scan XPS spectrum confirmed the presence of C, Ni, and S elements in the NiS$_2$/graphene hybrid composite. In the XPS analysis, binding energy (BE) referencing method is commonly performed with C 1*s* peak of adventitious carbon (AdC) to determine the chemical-state of specimens. Recent survey on XPS literature shows C 1*s* peak ($E_B^F$) position varied over a large range from 284.4 to 285.7 eV reliant on the substrate [36]. The high-magnification C 1*s* XPS spectrum was divided into two peaks (Fig. 6b) at

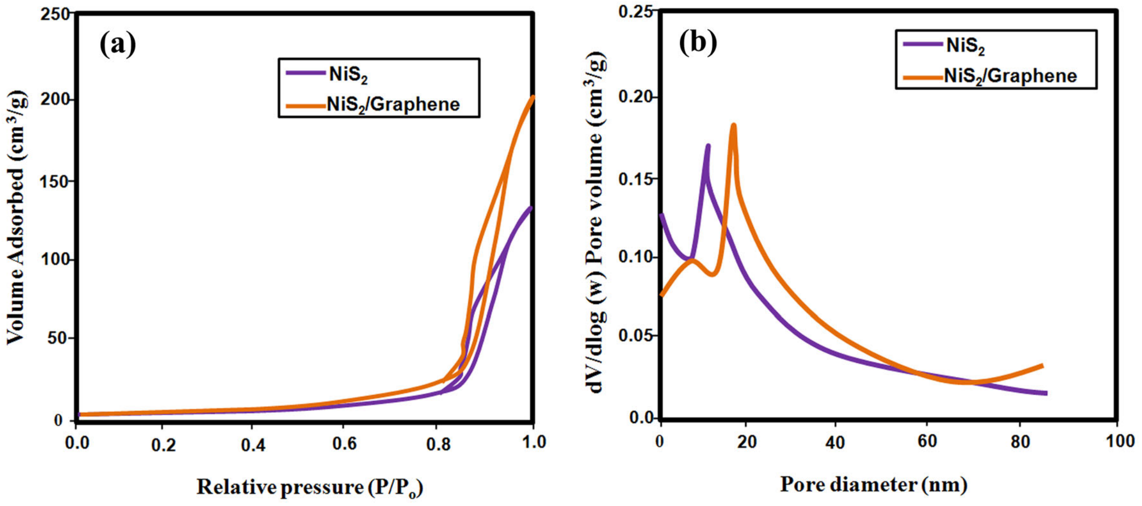

**Fig. 5** **a** N$_2$ adsorption and desorption analysis of graphene, NiS$_2$, NiS$_2$/G and **b** corresponding pore size distribution

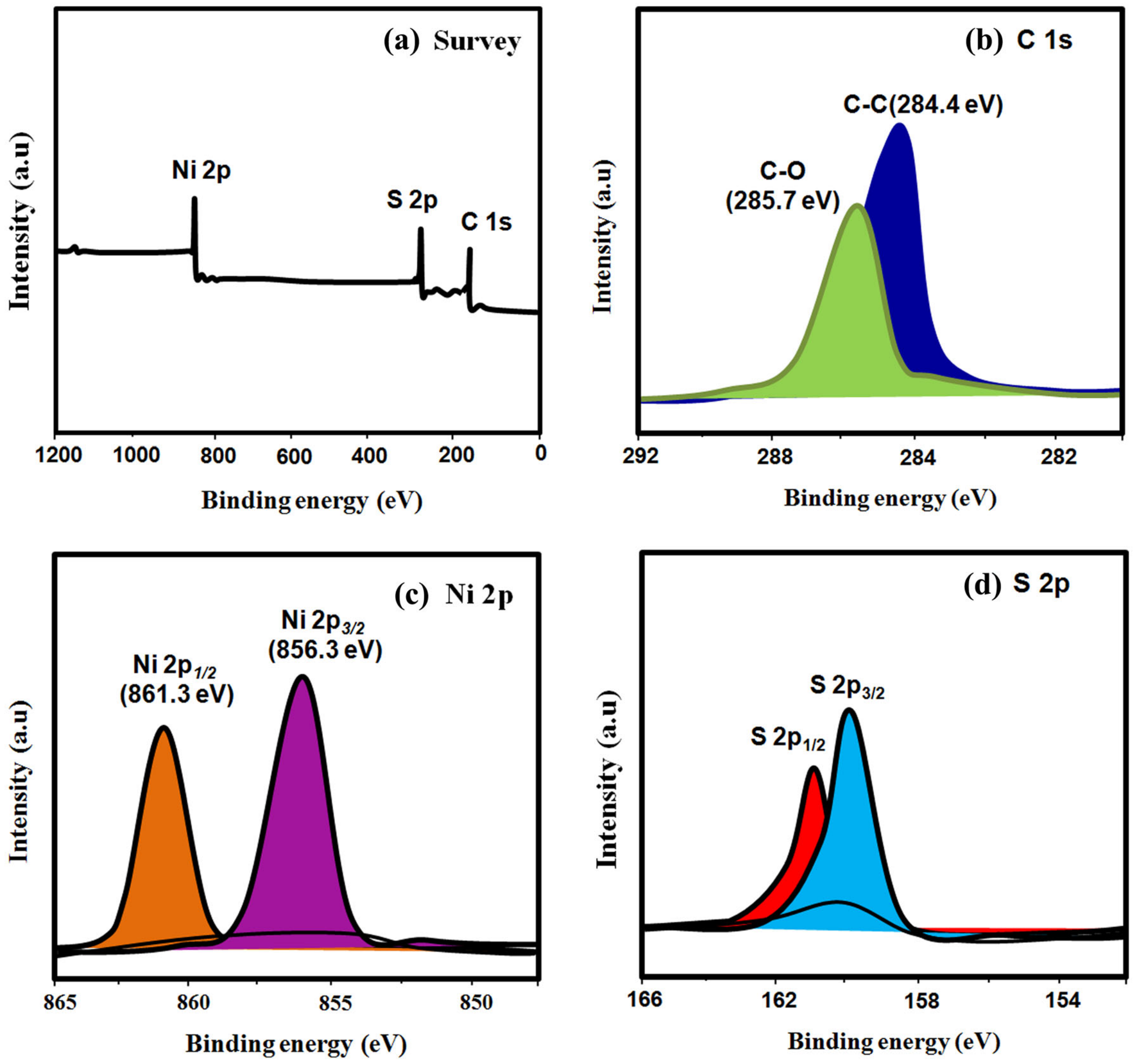

**Fig. 6** XPS of $NiS_2$/graphene **a** survey, **b** C 1*s*, **c** Ni 2*p* and **d** S 2*p*

285.3 eV, which could be assigned to the obvious adventitious carbon [37] and loaded graphitic carbon (C–C bonds) on the sample surface, and at 286.2 eV, which might originate from absorbed gaseous molecules (C–O bonds). The HR XPS peaks of Ni 2*p* spectrum located at 856.3 (Ni $2p_{3/2}$) and 861.6 eV (Ni $2p_{3/2}$) correspond to the dominant oxidation state of $Ni^{2+}$ (Fig. 6c). Additionally, S 2p peaks were located at 161.4 and 160.1 eV (Fig. 6d) with a spin–orbit separation of 1.2 eV, corresponding to sulfide in $NiS_2$ sample [38].

## 3.6 Gas-sensing test

The prepared sensor films were exposed to air atmosphere in order to find out the resistance behavior of the thin film sensors. The resistance of the sensor sample was measured as a function of temperature and the temperature is varied from 0 to 400 °C. Figure 7a shows the resistance of the graphene, $NiS_2$ and $NiS_2$/graphene composite sensor samples. At RT, the resistance values of graphene, $NiS_2$, and $NiS_2$/graphene composite sensors were found to be 34 KΩ, 45 KΩ and 57 KΩ, respectively. At 400 °C, the resistance values of graphene, $NiS_2$, and $NiS_2$/graphene composite sensors were found to be 63 KΩ, 84 KΩ and 112 KΩ, respectively. It was clear that the resistance of $NiS_2$/graphene is higher than pristine graphene and $NiS_2$, respectively. It can be seen that the resistance values of all the sensor sample drops around at 300 °C. Hence, it was concluded that 300 °C was optimum temperature of the sensor

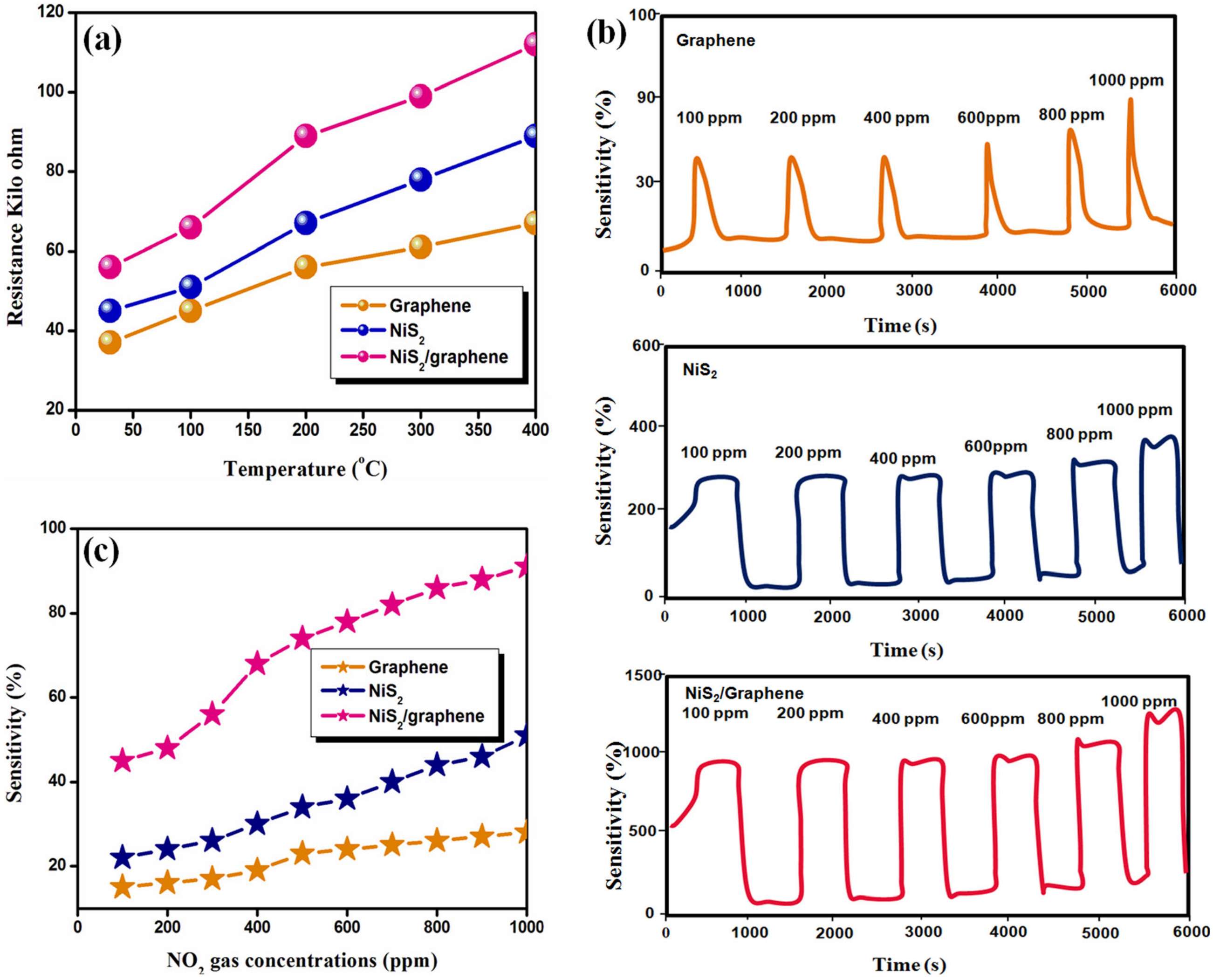

**Fig. 7** **a** Resistance variation as a function of temperature, **b** Dynamic response of $NO_2$ gas and **c** sensitivity plot of all the sensor sample

samples. Therefore, the $NO_2$ gas-sensing performance of the sensor samples was measured at 300 °C with different concentration. The $NO_2$ gas concentration was varied from 100 to 1000 ppm, and the dynamic response of the sensor samples were displayed in Fig. 7b. It was clear that sensing response of $NiS_2$/graphene composite sensor showed superior than compared with graphene and $NiS_2$. The sensor response is calculated using $S\ (\%) = \Delta R/R \times 100$, where $\Delta R$ is a difference between the gas and air resistance; $R$ is the gas resistance [32]. Figure 7c shows the sensitivity plot of the sensor films. The $NiS_2$/Graphene sensor had the highest sensitivity (97%) to $NO_2$ gas at a concentration of 1000 ppm, where as pristine graphene and NiS2 was found to be 28% and 51%, respectively. The response and recovery time calculated from the dynamic response plot of Fig. 8a–c indicates a very short response time of 19 s and a recovery time of 37 s for the $NiS_2$/-graphene composite at 1000 ppb concentrations. The response and recovery times for the graphene sensor are 61 s & 48 s and 51 s & 37 s for the $NiS_2$ sensor. The $NO_2$ gas sensing parameters of the sensor sample was summarized in Table 1. Surprisingly, the $NiS_2$/graphene sensor has a faster response time than the other two sensors, but a longer recovery time. The reason for this is the $NiS_2$/graphene sensor's huge specific surface area and many pores, which are favourable for gas diffusion and monitoring reactions. Due to the presence of water vapour in the exhaust gas, such sensors are typically used in humid conditions. We evaluated the influence of humidity on $NO_2$ detection with sensors at 300 °C based on our earlier data. The $NO_2$ gas-sensing parameters of the

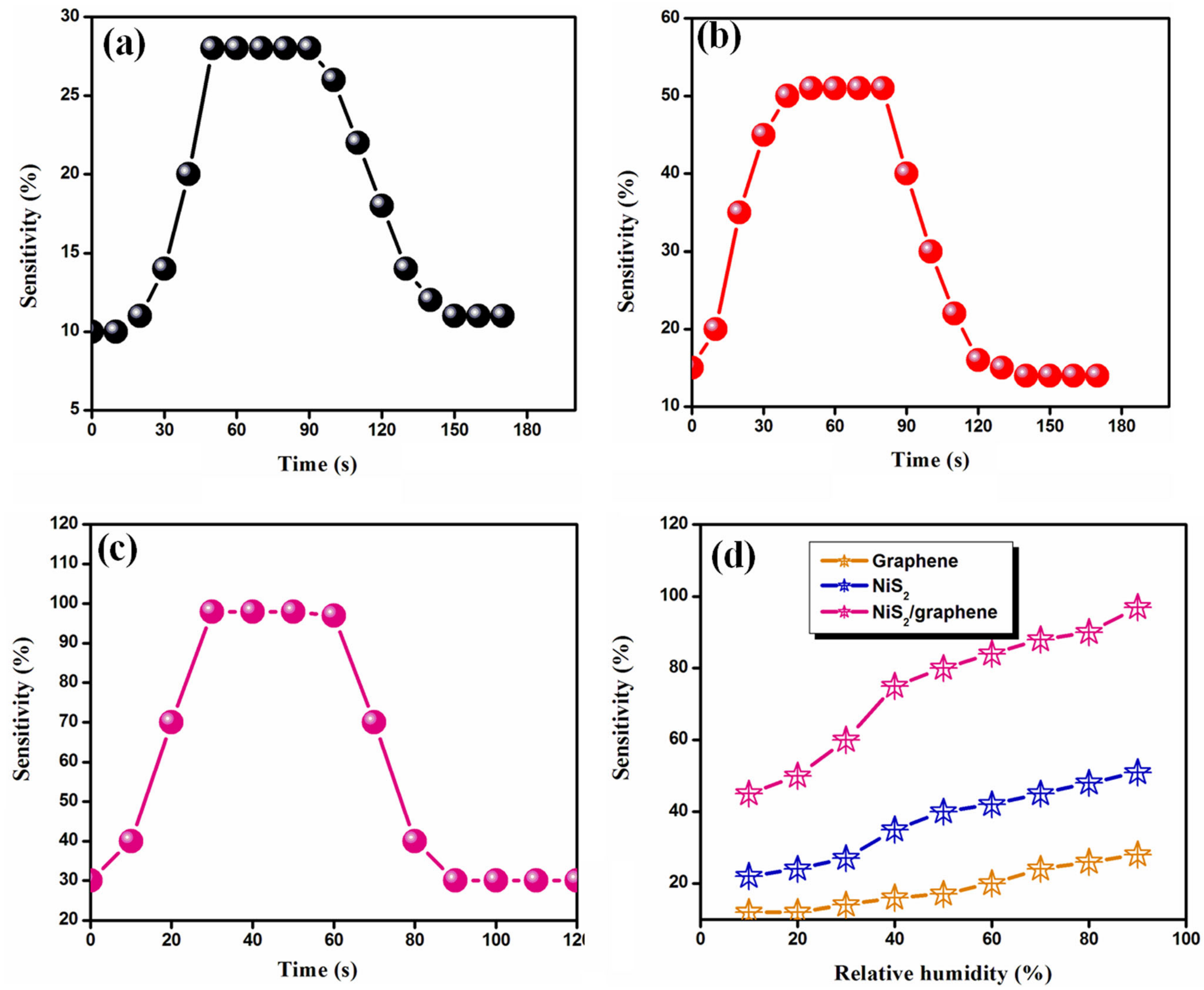

**Fig. 8** Response and recovery time of **a** graphene, **b** $NiS_2$, **c** $NiS_2$/G, **d** Sensing response as a function of humidity

**Table 1** Gas-sensing parameters of the sensor samples

| Samples | Sensitivity (%) | Response time (s) | Recovery time (s) |
|---|---|---|---|
| Graphene | 28 | 61 | 48 |
| $NiS_2$ | 51 | 51 | 37 |
| $NiS_2$/graphene | 97 | 34 | 39 |

sensors was further evaluated with presence of various humidity levels (0–90%) at 300 °C and the result plot is shown in Fig. 8d. As shown in Fig. 8d, the sensor signal is drop gradually with the increase of humidity level form 10% to 90%. The composite sensor sening performance was found to be 96, 76, and 70% with the relative humididty level of 30%, 60% and 90%, respectively. Gas sensors must have not only great sensitivity and repeatability, but also strong selectivity to the target gas for practical applications. As a result, the response of the sensor with graphene, $NiS_2$, and $NiS_2$/graphene thin film sensors toward various toxic gases was investigated in order to evaluate its selectivity at the optimum working temperature (300 °C) (e.g., $CO_2$, $H_2$, $NH_3$ and $CH_4$). The bar diagram (Fig. 9a–c clearly illustrates that all sensors exposed to $NO_2$ gas have a higher sensing response than other gases. As a result, the sensor has a high selectivity for $NO_2$ gas as compared to other gases. The long-term stability is

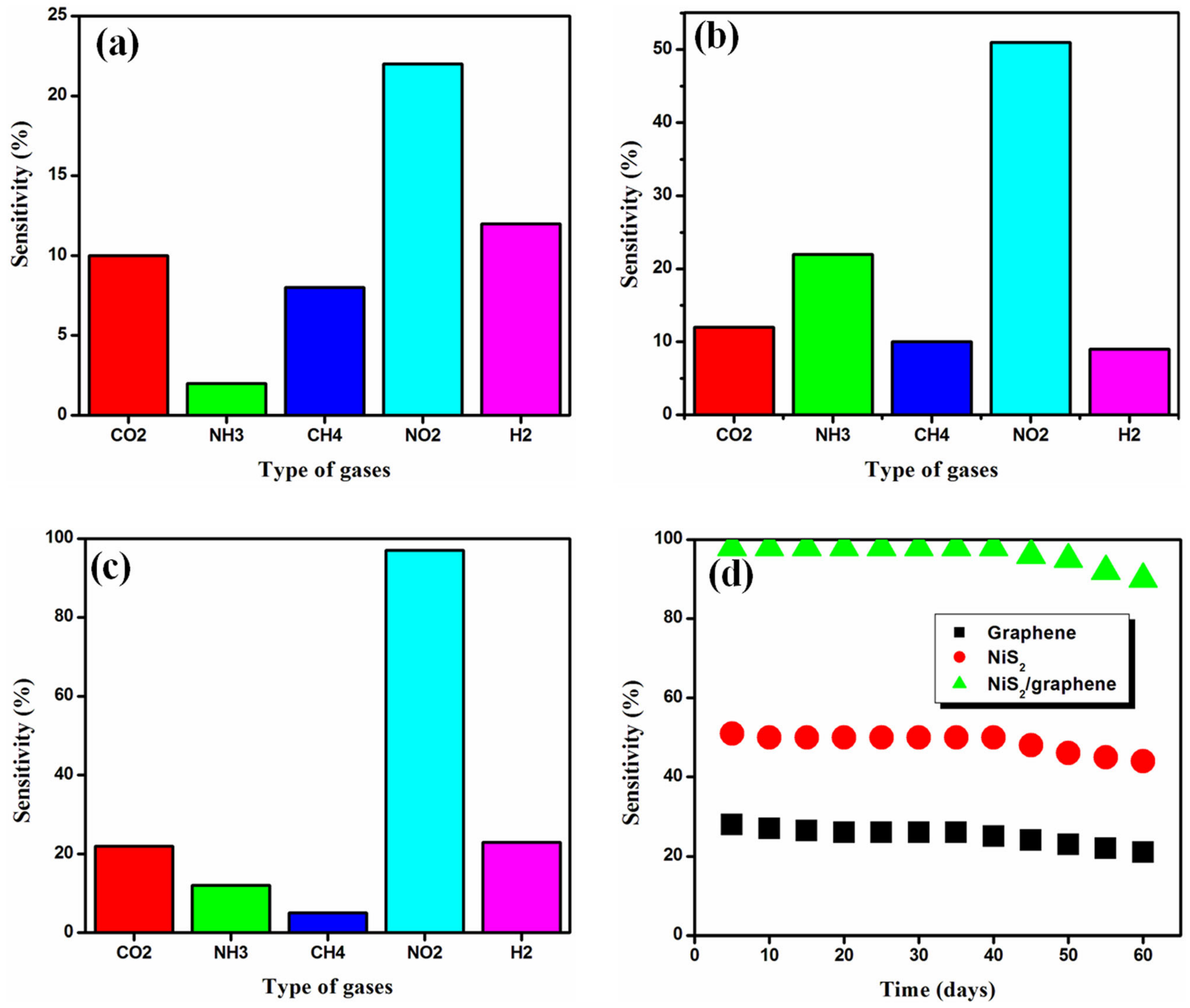

**Fig. 9** **a** Long-term stability; Selectivity response curve of **b** graphene, **c** $NiS_2$, **d** $NiS_2$/G

plotted in Fig. 9d. It was clear evident that the $NO_2$ response was did not change noticeably for the period of 45 days at a testing with 100 ppm level of $NO_2$ gas. Table 2 compares the $NO_2$ gas sensing properties of the $NO_2$ gas sensor suggested in this paper with those reported elsewhere in the literature [33–35, 39–41]. In order to investigate the effect of graphene incorporation on the photo conducting properties of $NiS_2$, the current–voltage (I–V) characteristics were recorded. Fig. S5 represents the I–V

**Table 2** Comparison of gas-sensing performances of the $NiS_2$/graphene composite sensor toward $NO_2$ with previous works

| Sensing materials | Sensor type | $NO_2$ (ppm) | Sensitivity | Refs. |
|---|---|---|---|---|
| $MoS_2$ | Chemiresistor | 100 | 58 | [33] |
| $MoS_2$ | Chemiresistor | 150 | 78 | [34] |
| $SnO_2$/graphene | Chemiresistor | 200 | 28 | [35] |
| $MoS_2$/graphene | Chemiresistor | 200 | 31 | [39] |
| $SnS_2$ | Chemiresistor | 200 | 27 | [40] |
| $MoS_2$/ZnO | Chemiresistor | 200 | 35 | [41] |
| $NiS_2$/graphene | Chemiresistor | 100 | 97 | This work |

characteristics of pure $NiS_2$ and $NiS_2$/graphene composite films for UV light power density of 750 mW/$cm^2$. The linear nature of I–V curve suggests that $NiS_2$ and $NiS_2$/graphene have ohmic contact. Graphene nano-sheets facilitate the carrier transportation in composite films with $NiS_2$. With the addition of graphene, the $NiS_2$/graphene composite films show enhanced current production under UV irradiation ($\lambda$ = 374 nm). This can be attributed to the increase in carrier concentration with incorporation of graphene as estimated from optical measurements. In the case of $NiS_2$/graphene, the generated charge carriers under illumination travel through the highly conductive graphene layer which is embedded between the $NiS_2$ particles (morphology as observed in SEM and TEM images). A schematic illustration of sensing mechanism is shown in Fig. 10. For bare graphene layer, as shown in Fig. 10a, the electrons transfer from reducing $NO_2$ gas molecules to p-type graphene nanosheets and result in a decrease of charge carriers concentration (the resistance increases). After an appropriate amount of graphene nanosheets are deposited on the surface of $NiS_2$ nanoparticles film, we suggest two kinds of adsorption sites, being related to graphene nanosheets surface and $NiS_2$/graphene interfaces, exist in bilayer thin film, in which the latter one might be responsible for the enhancement of sensing properties compared with pure graphene film. It is noteworthy that although $O_2^-$ could be produced on the surface of $NiS_2$ nanoparticles even at room temperature (see Fig. 10b), the catalytic oxidation ability of $O_2^-$ is not powerful enough to convert $NO_2$ as the final product ($N_2$ and O) when the temperature is lower than 373 K. However, since the work function of p-graphene (4.75 eV) is lower than that of n-$NiS_2$ (5.20 eV), a considerable amount of local accumulation heterojunctions at interfaces between graphene nanosheets and $NiS_2$ nanoparticles might be formed at $NiS_2$/graphene interfaces, in which more holes and electronics could accumulate in graphene and $NiS_2$ regions of heterojunction, respectively, as shown in the magnified view of Fig. 10b. In the present case, graphene becomes more p-type than the original state, and thus, the energy barrier between absorbed $NO_2$ molecules and graphene is further reduced, resulting in the higher response values and shorter response times. The increase of $NO_2$ sensor response in the presence of humidity can be explained as follows: in the absence of humidity, only adsorbed oxygen occupies all available active sites on the surface of the sensing layer, whereas in the presence of humidity, some active sites will be occupied by water molecules. In other words, in dry condition, more surface adsorbed oxygen implies that more target gas will react with the sensing material, and thus,

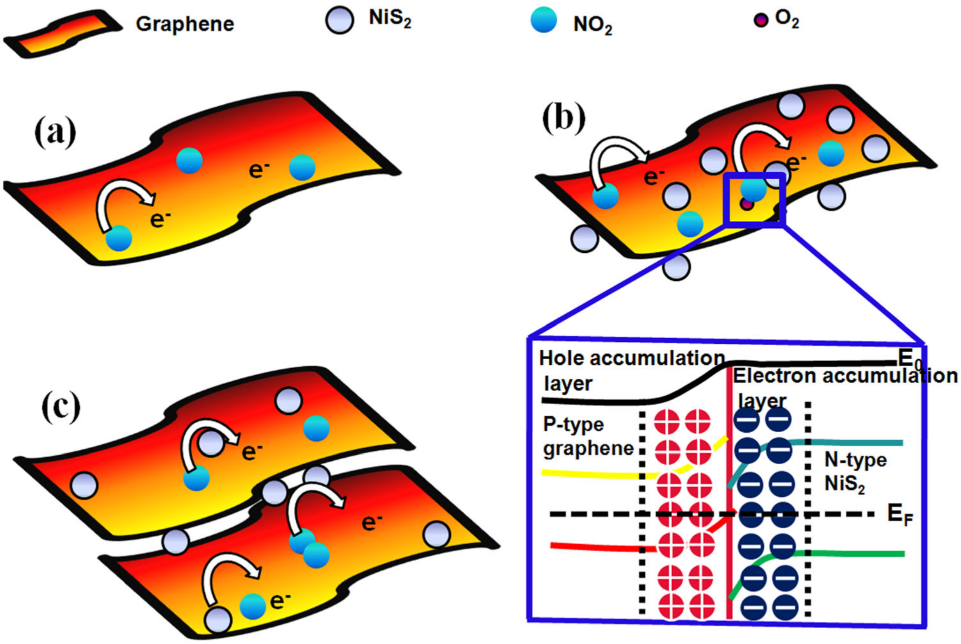

**Fig. 10** Schematic illustration of $NO_2$-sensing mechanism of **a** graphene and **b**, **c** graphene/$NiS_2$ film sensor, in which **b** and **c** shows the adsorption sites of graphene/$NiS_2$ film with proper and excess rGO amount, respectively, and the magnified view in (**b**) is the formed accumulation heterojunctions at the interface

enhance the sensor response as a result of the reaction between the target gases with the adsorbed oxygen. However, the observed increase of $NO_2$-selectivity can be ascribed to the achievement of higher affinity between –OH species and $NO_2$ than other gases. As observed, in the presence of water molecules, $NO_2$ will be readily adsorbed on the surface than other gases because of the fact that the Van der Waal forces between O–H and $NO_2$ are stronger than those between O–H and CO. This will lead to the enhancement of $NO_2$-absorption on the sensing layer than that of other gases resulting in better selectivity toward $NO_2$.

## 4 Conclusion

In conclusion, pure $NiS_2$ and $NiS_2$/graphene hybrid thin film was successfully deposited by a thermal spray-CVD technique. The sensing properties of the sensor having this $NiS_2$ and $NiS_2$/graphene film as sensing material were tested between RT and 400 °C toward various gases (e.g., $CO_2$, $NH_3$, $CH_4$, $NO_2$ and $H_2$). The $NiS_2$ gas sensor responded with a 28% change upon being exposed to 100 ppm of $NO_2$, while the response of the $NiS_2$/graphene device reached 97% when exposed to the same $NO_2$ concentration. The results show that the addition of the $NiS_2$ nanoparticles to the graphene matrix can improve the sensing performances: firstly, by increasing the sensing response towards $NO_2$ and secondly by enhancing the selectivity. The introduction of $NiS_2$ nanoparticles seems mainly affecting the film morphology. $NiS_2$ nanoparticles prevent graphene sheets from restacking, thus increasing specific surface area. In addition, the preferential placement of the $NiS_2$ nanoparticles clusters along the flake edges fosters the faster interaction of the $NO_2$ with the sp2 carbon atoms of the graphene sheets. This finally leads to the enhancement of surface properties such as catalytic activity or surface adsorption, essential properties to produce chemical sensors with superior performances. This work demonstrates a promising gas-sensing platform based on $NiS_2$/-graphene heterostructures and could also have implications for broader applications that utilize the unique electronic properties of hybrid 2D graphene/TMDCs heterostructures.

## Author contributions

RS, AG, BAA: study conceptualization and writing (original draft) the manuscript. SM, JD: data curation, formal analysis and writing (review & editing), and funding acquisition and project administration.

## Funding

There is no funding received from any other institutions.

## Data availability

The data that support the findings of this study are available from the corresponding author, upon reasonable request.

## Declarations

**Conflict of interest** The authors declare they have no conflicts of interest.

**Supplementary Information:** The online version contains supplementary material available at https://doi.org/10.1007/s10854-022-09101-z.

## References

1. N. Yamazoe, N. Miura, Environmental gas sensing. Sens. Actuators B **20**, 95–102 (1994)
2. L. Duk-Dong, L. Dae-Sik, Environmental gas sensors. IEEE Sens. J. **1**, 214–224 (2001)
3. G.F. Fine, L.M. Cavanagh, A. Afonja, R. Binions, Metal oxide semi-conductor gas sensors in environmental monitoring. Sensors **10**, 5469 (2010)
4. K. Wetchakun, T. Samerjai, N. Tamaekong, C. Liewhiran, C. Siriwong, V. Kruefu et al., Semiconducting metal oxides as sensors for environmentally hazardous gases. Sens. Actuators B **160**, 580–591 (2011)
5. D. Chen, Yu. Wencheng, L. Wei, J. Ni, H. Li, Y. Chen, Y. Tian, S. Yan, L. Mei, J. Jiao, High sensitive room temperature $NO_2$ gas sensor based on the avalanche breakdown induced by Schottky junction in $TiO_2$–$Sn_3O_4$ nanoheterojunctions. J. Alloy. Compd. **912**, 165079 (2022)
6. S. Rani, M. Kumar, H. Sheoran, R. Singh, V. Nand Singh, Rapidly responding room temperature $NO_2$ gas sensor based on SnSe nanostructured film. Mater. Today Commun. **30**, 103135 (2022)

7. H.S. Hong, N.H. Ha, D.D. Thinh, N.H. Nam, N.T. Huong, N.T. Hue, T.V. Hoang, Enhanced sensitivity of self-powered $NO_2$ gas sensor to sub-ppb level using triboelectric effect based on surface-modified PDMS and 3D-graphene/CNT network. Nano Energy **87**, 106165 (2021)
8. A.A. Kabure, B.S. Shirke, S.R. Mane, K.M. Garadkar, Microwave-assisted sol-gel synthesis of $CeO_2$–NiO nanocomposite based $NO_2$ gas sensor for selective detection at lower operating temperature. J. Indian Chem. Soc. **99**, 100369 (2022)
9. H.S. Hong, N.H. Phuong, N.T. Huong, N.H. Nam, N.T. Hue, Highly sensitive and low detection limit of resistive $NO_2$ gas sensor based on a $MoS_2$/graphene two-dimensional heterostructures. Appl. Surf. Sci. **492**, 449–454 (2019)
10. Y. Su, G. Xie, H. Tai, S. Li, B. Yang, S. Wang, Q. Zhang, H. Du, H. Zhang, X. Du, Y. Jiang, Self-powered room temperature $NO_2$ detection driven by triboelectric nanogenerator under UV illumination. Nano Energy **47**, 316–324 (2018)
11. S. Guo, D. Yang, S. Zhang, Q. Dong, B. Li, N. Tran, Z. Li, Y. Xiong, M.E. Zaghloul, Development of a cloud-based epidermal $MoSe_2$ device for hazardous gas sensing. Adv. Funct. Mater. **29**, 1900138 (2019)
12. H. Li, W. Xie, B. Liu, C. Wang, Y. Wang, X. Duan, Q. Li, T. Wang, Gas modulating effect in room temperature ammonia sensing. Sensor. Actuator. B **242**, 404 (2017)
13. N. Joshi, T. Hayasaka, Y. Liu, H. Liu, O.N. Oliveira, L. Lin, A review on chemiresistive room temperature gas sensors based on metal oxide nanostructures, graphene and 2D transition metal dichalcogenides. Microchim. Acta **185**, 213 (2018)
14. G. Korotcenkov, Gas response control through structural and chemical modification of metal oxide films: state of the art and approaches. Sensor. Actuator. B **107**, 209 (2005)
15. Q. He, S. Wu, Z. Yin, H. Zhang, Graphene-based electronic sensors. Chem. Sci. **3**, 1764 (2012)
16. S. Yang, C. Jiang, S.-H. Wei, Gas sensing in 2D materials. Appl. Phys. Rev. **4**, 021304 (2017)
17. L. Calderón-Garcidueñas, B. Azzarelli, H. Acuna, R. Garcia, T.M. Gambling, N. Osnaya, S. Monroy, M.R. Del Tizapantzi, J.L. Carson, A. Villarreal-Calderon, B. Rewcastle, Air pollution and brain damage. Toxicol. Pathol. **30**, 373–389 (2002)
18. Y. Liu, J. Parisi, X. Sun, Y. Lei, Solid-state gas sensors for high temperature applications—a review. J. Mater. Chem. A **2**, 9919–9943 (2014)
19. A. Afzal, N. Cioffi, L. Sabbatini, L. Torsi, NOx sensors based on semiconducting metal oxide nanostructures: progress and perspectives Sens. Actuators B **171**, 25–42 (2012)
20. M.W. Nomani, R. Shishir, M. Qazi, D. Diwan, V. Shields, M. Spencer, G.S. Tompa, N.M. Sbrockey, G. Koley, Highly sensitive and selective detection of $NO_2$ using epitaxial graphene on 6H-SiC. Sensor. Actuator. B **150**, 301 (2010)
21. G. Lu, S. Park, K. Yu, R.S. Ruoff, L.E. Ocola, D. Rosenmann, J. Chen, Toward practical gas sensing with highly reduced graphene oxide: a new signal processing method to circumvent run-to-run and device-to-device variations. ACS Nano **5**, 1154 (2011)
22. D.A.C. Brownson, D.K. Kampouris, C.E. Banks, An overview of graphene in energy production and storage applications. J. Power Sources **196**, 4873–4885 (2011)
23. M.D. Stoller, S. Park, Y. Zhu, J. An, R.S. Ruoff, Graphene-based ultracapacitors. Nano Lett. **8**, 3498–3502 (2008)
24. G.J. Hu, C. Xu, Z.H. Sun, S.G. Wang, H.M. Cheng, F. Li, W.C. Ren, 3D graphene foam- reduced-graphene-oxide hybrid nested hierarchical networks for high performance Li–S batteries. Adv. Mater. **28**, 1603–1609 (2016)
25. M.M. Rahman, J. Ahmed, A.M. Asiri, I.A. Siddiquey, M.A. Hasnat, Development of 4-methoxyphenol chemical sensor based on $NiS_2$ -CNT nanocomposites. J. Taiwan Inst. Chem. Eng. **000**, 1–9 (2016)
26. J.S. Anand, R.K.M. Rajan, A.A.M. Zaidan, Electro synthesized $NiS_2$ thin films and their optical and semiconductor studies. Rep. Electrochem. **3**, 25–29 (2013)
27. L.P. Mgabi, B.S. Dladla, M.A. Malik, S.S. Garje, J. Akhtar, N. Revaprasadu, Deposition of cobalt and nickel sulfide thin films from thio- and alkylthiourea complexes as precursors via the aerosol assisted chemical vapour deposition technique. Thin Solid Films **564**, 51–57 (2014)
28. X. Ke, G. –z. Hao, Y. –b. Rong, X. Zhou, J. Liu, L. Xiao, W. Jian, A facile approach to the hydrothermal synthesis of graphene Proceedings of the 16th International Conference on Nanotechnology Sendai, Japan, August 22–25, 2016
29. R. Siburian, H. Sihotanh, S. LumbanRaja, M. Supeno, C. Simanjuntak, New route to synthesize of graphene nano sheets. Orient. J. Chem. **34**, 182–187 (2020)
30. S.L. Yang, H.B. Yao, M.R. Gao, S.H. Yu, Monodisperse cubic pyrite $NiS_2$ do- decahedrons and microspheres synthesized by a solvothermal process in a mixed solvent: thermal stability and magnetic properties. Cryst. Eng. Commun. **11**, 1383 (2009)
31. C. Marini, B. Joseph, S. Caramazza, F. Capitani, M. Bendele, M. Mitrano, D. Chermisi et al., Local disorder investigation in $_{NiS2}$-XSex using raman and Ni K-Edge X-ray absorption spectroscopies. J. Phys. Condens. Mater. **26**, 1–8 (2014)
32. X. Li, J. Wang, D. Xie, Xu. Jianlong, Yi. Xia, L. Xiang, S. Komarneni, Reduced graphene oxide/$MoS_2$ hybrid films for room-temperature formaldehyde detection. Mater. Lett. **189**, 42–45 (2017)
33. M. Donarelli, S. Prezioso, F. Perrozzi, F. Bisti, M. Nardone, L. Giancaterini et al., Response to $NO_2$ and other gases of

resistive chemically exfoliated $MoS_2$-based gas sensors. Sens. Actuators B **207**, 602–613 (2015)

34. L. Yu, F. Guo, S. Liu, J. Qi, M. Yin, B. Yang, Z. Liu, X. Fan, Hierarchical 3D flower-like $MoS_2$ spheres: post-thermal treatment in vacuum and their $NO_2$ sensing properties. Mater. Lett. **183**, 122–126 (2016)
35. N. Tammanoon, A. Wisitsoraat, C. Sriprachuabwong, D. Phokharatkul, A. Tuantranont, S. Phanichphant, C. Liewhiran, Ultrasensitive $NO_2$ sensor based on ohmic metal-semiconductor interfaces of electrolytically exfoliated graphene/flame-spray-made $SnO_2$ nanoparticles composite operating at low temperatures. ACS Appl. Mater. Interfaces. **7**, 24338–24352 (2015)
36. G. Greczynski, L. Hultman, X-ray photoelectron spectroscopy: towards reliable binding energy referencing. Prog. Mater. Sci **107**, 100591 (2019)
37. G. Greczynski, L. Hultman, Reliable determination of chemical state in x-ray photoelectron spectroscopy based on sample-work-function referencing to adventitious carbon: resolving the myth of apparent constant binding energy of the C 1s peak. Appl. Surf. Sci. **451**, 99–103 (2018)
38. J. He, L. Chen, Z.Q. Yi, C.T. Au, S.F. Yin, CdS nanorods coupled with $WS_2$ nanosheets for enhanced photocatalytic hydrogen evolution activity. Ind. Eng. Chem. Res. **55**, 8327–8333 (2016)
39. S. Cui, Z. Wen, X. Huang, J. Chang, J. Chen, Stabilizing $MoS_2$ nanosheets through $SnO_2$ nanocrystal decoration for high-performance gas sensing in air. Small **11**, 2305–2313 (2015)
40. J.Z. Ou, W. Ge, B. Carey, T. Daeneke, A. Rotbart, W. Shan, Y. Wang et al., Physisorption-based charge transfer in two-dimensional $SnS_2$ for selective and reversible $NO_2$ gas sensing. ACS Nano **9**, 10313–10323 (2015)
41. Y. Han, Da. Huang, Y. Ma, G. He, Hu. Jun, J. Zhang, Hu. Nantao, Su. Yanjie, Z. Zhou, Y. Zhang, Z. Yang, Design of hetero-nanostructures on $MoS_2$ nanosheets to boost $NO_2$ room-temperature sensing. ACS Appl. Mater. Interfaces **10**, 22640–22649 (2018)